



LAWRENCE
LIVERMORE
NATIONAL
LABORATORY

Detection of Off-normal Images for NIF Automatic Alignment

J. V. Candy, A. A. S. Awwal, W. A. McClay, S. W.
Ferguson, S. C. Burkhart

July 15, 2005

SPIE Optics & Photonics 2005
San Diego, CA, United States
July 31, 2005 through August 4, 2005

Disclaimer

This document was prepared as an account of work sponsored by an agency of the United States Government. Neither the United States Government nor the University of California nor any of their employees, makes any warranty, express or implied, or assumes any legal liability or responsibility for the accuracy, completeness, or usefulness of any information, apparatus, product, or process disclosed, or represents that its use would not infringe privately owned rights. Reference herein to any specific commercial product, process, or service by trade name, trademark, manufacturer, or otherwise, does not necessarily constitute or imply its endorsement, recommendation, or favoring by the United States Government or the University of California. The views and opinions of authors expressed herein do not necessarily state or reflect those of the United States Government or the University of California, and shall not be used for advertising or product endorsement purposes.

Detection of Off-normal images for NIF Automatic Alignment

James V. Candy*, Abdul A. S. Awwal, Wilbert A. McClay III, S. Walter Ferguson and Scott Burkhart

University of California, Lawrence Livermore National Laboratory, P.O. Box 808, L-495, (L-156*)
Livermore, CA 94526

ABSTRACT

One of the major purposes of National Ignition Facility at Lawrence Livermore National Laboratory is to accurately focus 192 high energy laser beams on a nanoscale (mm) fusion target at the precise location and time. The automatic alignment system developed for NIF is used to align the beams in order to achieve the required focusing effect. However, if a distorted image is inadvertently created by a faulty camera shutter or some other opto-mechanical malfunction, the resulting image termed “off-normal” must be detected and rejected before further alignment processing occurs. Thus the off-normal processor acts as a preprocessor to automatic alignment image processing. In this work, we discuss the development of an “off-normal” pre-processor capable of rapidly detecting the off-normal images and performing the rejection. Wide variety of off-normal images for each loop is used to develop the criterion for rejections accurately.

1. INTRODUCTION

The alignment of large operative, high power short pulse, laser systems is a complex and critical process requiring precise and accurate measurements. If beam alignment is not performed in an optimal manner, costly optics could be damaged disrupting an entire experiment. Early alignment systems proved inadequate due to inherent uncertainties and lack of reliability. Therefore, contemporary imaging systems evolved based on using video cameras to image and align the beam.¹⁻¹⁰ This approach estimates the current beam position from the image, adjusts mirrors relative to an accurate reference measurement of physical beam center and attempts to minimize the deviation between them.²⁻¹⁰ Current systems employ the same basic principle, but utilize much improved high-resolution video cameras and more accurate position control systems.¹⁰ However, even with these improved systems, should an anomalous or equivalently “off-normal” image occur due to component malfunctions (sticky mirror, stepping motor failure, component failure, etc.), the current system will still attempt to perform its alignment function unless there is some method to detect, classify and reject the erroneous image prior to position imaging and eventual control loop adjustments. This paper is concerned not only with detecting and classifying off-normal images, prior to processing, but also rejecting any anomalous images during laser system operations. In this paper, we present a suite of operations under the above-mentioned constraints to detect, classify and reject any off-normal images prior to processing, thereby, enabling a minimal distortion of pulsed laser operations.

High power, tightly focused laser beams are required to achieve successful ignition and therefore fusion at the Lawrence Livermore National Laboratory (LLNL) National Ignition Facility (NIF).¹¹ The beams simultaneously focus precisely on a nanoscale target capsule to succeed. Therefore, there are a large number of alignment measurements that must be performed along the NIF beam lines to assure that the pointing and alignment control system centers the beam in order to provide the maximum energy on the fusion target located in the associated chamber.¹¹⁻¹³ An automatic alignment (AA) system was designed and implemented to assure successful deployment of the high energy beam in each of the 192 beam lines. Initially, only four beam lines were constructed and aligned manually by well-trained operators and sophisticated diagnostic tools; however, a fully automated system is close to completion. Hence, the requirement of an “off-normal” detection implementation scheme is crucial.

Let us briefly describe the operation of the alignment procedure to emphasize the importance of the screening. The alignment images are acquired from a charge-coupled device (CCD) imaging camera producing both noisy reference and measurement images. The precise reference image is used to provide the desired fiducial that is used by the alignment system. Corrections to align the measured image with the reference is accomplished by using the dedicated control loops that adjust pointing mirror stepping motors until the deviations between both reference and measured positions are within acceptable limits.¹³⁻¹⁴

The ideal approach to perform the detection, classification and off-normal rejection system is based on a very simple concept: “reduce the dense pixel image to a simple or set of simple functions that capture the essential features of the alignment pattern or inherent structure.

We develop a variety of such transformations in Sec. 2. In Sec. 3 a set of ideal ensemble averaged images are transformed and detected to demonstrate the various approaches. Results from actual NIF off-normal images are discussed next evaluating their overall performance and finally summarize the results and discuss future work.

2. IMAGE TRANSFORMATIONS FOR OFF-NORMAL DETECTION

In this section we begin by examining some of the simpler alignment images to motivate our approach and then investigate the more technical. First, we consider the cases of black and white images, created by faulty shutters, illumination, hardware failures etc. The approach that we take to design the processor is based on classification/detection theory. We decided to construct the *off-normal classifier/detector* as a two-stage processor: the first is a Bayesian-type classifier to determine the class the image belongs based on its unique probability mass function (PMF) features, while the second stage can be considered a feature detector based on tolerance parameters that must be satisfied for successful operation of the alignment system.¹⁵⁻¹⁶

The overall question that must be answered by the pre-processor is

“GIVEN a noisy measured image, DETERMINE whether it is good or bad. IF good, pass it to the imaging alignment algorithm or IF bad, reject it.”

Once the decision is made, the image is processed accordingly.

In this paper we will develop the concept of a classifier/detector based on transforming the measured 2D image to generate meaningful 1D features. The basic structure is shown in Fig. 1 below.

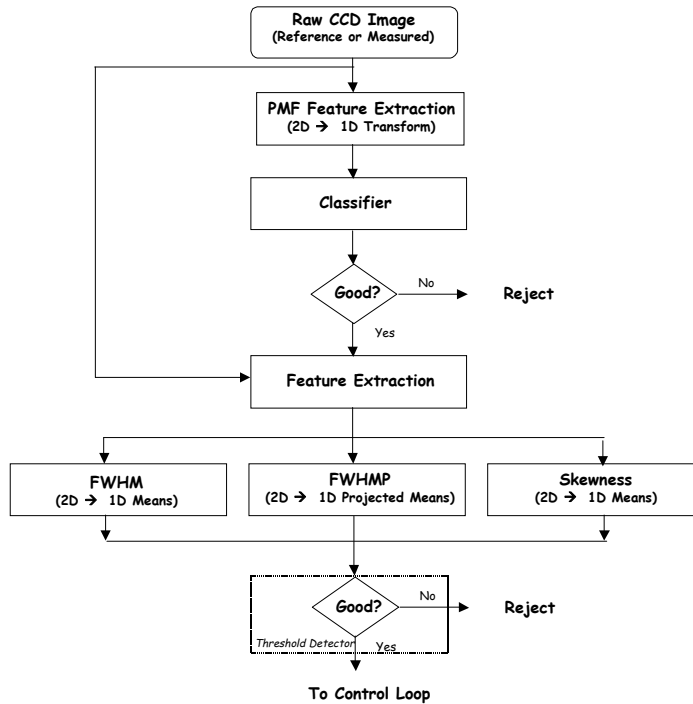


Fig. 1. NIF Off-Normal Image Classification/Detection: Classification and Detection stages.

Once the raw NIF image data (reference or measured image) is captured by the CCD camera, it is transformed, $2D \rightarrow 1D$ to generate a set of features that can be used for classification/detection. Because of the likelihood of the occurrence of black, white or noisy images, these are processed first. Should the image be accepted as “good”, it is passed on to a second set of detectors which again perform a variety of $2D \rightarrow 1D$ transformations creating decision functions which can be tested against a prescribed threshold based on the characteristics of the expected image. Should the image be passed again, it is sent to the actual imaging algorithm for eventual position estimation (e.g. centroiding).

First, we choose to use the probability mass function as a means of generating our desired feature sets for the black and white problem. Once they are generated then the next step is to extract a subset of the features to be used for overall classification of incoming image.

A. Classification Approach

Let, $I(x,y)$, represent our measured NIF image (reference or alignment). From the data we generate a set of features that uniquely characterize the particular image. We can represent a number of features by the vector, $\mathbf{f} \in R^{N_f \times 1}$ for our problem. Recall that a feature is a subset of the measured data image that is used for classification. Feature selection is a methodology to select the salient features characterizing the particular data image. We choose to transform the image to a probability mass function using a histogram estimator in the first stage. From the histogram we then extract the features. Once extracted, they are processed by a classifier. For our processor we choose to use a *Bayesian-type classifier*.¹⁴

1. NIF Classifier Design

In this section we develop the classifier used as the part of the preprocessor for NIF alignment images. The approach follows the paradigm that the image is transformed to an estimate of a 1D PMF (2D \rightarrow 1D). It is based on identifying and extracting a unique set of features for the most prevalent set of undesirable images (e.g. all black pixels). Thus, a unique features, $\{f_k\}$, $k = 1, \dots, N_f$, from selected off-normal images are identified, extracted and classified. The features provide the direct input in a Bayesian-type classification scheme.

a. Feature Generation

Next we describe a transformation of the acquired image to another space for eventual feature extraction. One of the primary motivations for this approach is the need for real-time processing in this automatic alignment application. For our problem, we use the probabilistic features available in the estimated image intensity probability mass function, $p(a)$. For the estimator we use the histogram defined in terms of the intensity, a_n , such that

$$p(a = a_n) \approx \hat{H}(a_n) := \frac{N(a_n)}{N_T} \quad \text{for } n = 0, \dots, N_a - 1 \quad (1)$$

where $N(a_n)$ is the number of occurrences of intensity a in the n^{th} bin (e.g. a_{255} is the counts in the 255-intensity bin) and N_T is the total number of intensities available in the image or the number of pixels, N_a is determined by the number of bits available, that is, for our 8-bit images, $N_a = 2^{N_{\text{bits}}} = 256$ intensity values ranging from 0 to 255. For a given interval, say $[a_{n-1}, a_n]$, we have that

$$N_T = \sum_{n=0}^{N_a-1} N(a_n) \quad (2)$$

with a_0 the number of zero-intensity counts. The histogram is an estimate of the PMF, which can be used to estimate the probability of intensity values

$$\Pr(a) = \sum_n p(a = a_n) = \sum_n \hat{H}(a_n) \quad \text{for all } n \text{ such that } a_n \leq a \quad (3)$$

Clearly, if we desire the probability of the intensity taking on values in a given range, then using the histogram estimate, we have

$$\Pr(a_i \leq a \leq a_j) = \sum_{n=i}^j p(a_i \leq a \leq a_j) = \sum_{n=i}^j \hat{H}(a_n) \quad (4)$$

In essence, our data, the measured images has been transformed to a 1D-estimate of the PMF using the histogram. Next we must extract a set of features from the PMF that uniquely characterize common (bad) images we expect to encounter in our data sets.

b. Feature Extraction

We define the components of the feature vector, \mathbf{f} , by a set of probabilities that will uniquely characterize an image by a class. Currently, we are considering four major classes: white, black or noise, (We use seven classes in the actual classifier, since there are four types of *black* images we must consider in the NIF problem).that is,

$$C := \{C_1, C_2, C_3, C_4\} \text{ for } C_1 \rightarrow \text{White}; \text{ for } C_2 \rightarrow \text{Black}; \text{ for } C_3 \rightarrow \text{Noise}; \text{ for } C_4 \rightarrow \text{Valid Image} \quad (5)$$

Our images are modeled in terms of the features of their corresponding intensities, that is,

$$I(x, y) = \{a_n\}; \quad a_i < a_n < a_j, \quad n = 1, \dots, N_a \quad (6)$$

where the pixilated image is $I(x, y)$ for $x = 1, \dots, N_x; y = 1, \dots, N_y$ with set of intensities, $\{a_n\}$ bound by the prescribed interval $[a_i, a_j]$. Corresponding to this definition, we can define the probability that the intensity of the k^{th} -feature will occur in this interval as

$$\Pr(a_i < a < a_j) = p_k \quad (7)$$

We define this probability as a component of our feature vector, estimated by the histogram for each particular image that will be used in the classifier, that is,

$$f_k = \hat{p}_k = \sum_{n=i}^j \hat{H}(a_n) \quad (8)$$

where f_k is the k^{th} -component of the feature vector estimated by summing the histogram over the interval, $[a_i, a_j]$. The classifier is then constructed as discussed in the previous section based on the conditional probability of the feature vector, $\Pr(\mathbf{f} | C_\ell)$.

For our problem using an 8-bit image, we must define the various types of images that can occur in our NIF beam line and characterize or model them by their features in terms of the probability intervals. We start with the various classes of *black* images, since these represent the most prevalent type and are of high concern.

Black images are more difficult to characterize, since there are varieties of the image that must be accounted for in the feature vector. For instance, an “all black” or pure black image is simple in that all of its pixel intensities are zero, that is,

$$I(x, y) = 0 \quad \forall a_n; \quad \text{with } f_1 = \hat{p}_1 = \hat{H}(0) \quad \text{[PURE BLACK]} \quad (9)$$

Another type of black image we frequently encounter is called a “good black” image that is the most typical of the black class and is defined by

$$I(x, y) = a_n \quad \ni \quad 17 < a_n < 19 \quad \text{with } f_2 = \hat{p}_2 = \sum_{n=17}^{19} \hat{H}(a_n) \geq \tau_{\text{prob}} \quad \text{[GOOD BLACK]} \quad (10)$$

where τ_{prob} is a probability bound of expected performance (e.g. 0.98) for good classification.

On the other hand, a “bad black” image is one that should not occur imply a potential physical problem with the CCD camera. It is defined by

$$I(x, y) = a_n \ni 1 < a_n < 9 \text{ with } f_3 = \hat{p}_3 = \sum_{n=0}^9 \hat{H}(a_n) \geq \tau_{\text{prob}} \quad [\text{BAD BLACK}] \quad (11)$$

A “normal black” image is characterized by

$$I(x, y) = a_n \ni 10 < a_n < 26 \text{ with } f_4 = \hat{p}_4 = \sum_{n=10}^{26} \hat{H}(a_n) \geq \tau_{\text{prob}} \quad [\text{NORMAL BLACK}] \quad (12)$$

A white image is defined by the property that its intensity is given by

$$I(x, y) = a_n \ni 225 < a_n < 255 \text{ with } f_5 = \hat{p}_5 = \sum_{n=225}^{255} \hat{H}(a_n) \quad [\text{WHITE}] \quad (13)$$

which means that the white image intensities range from [225,255] and its feature (probability) is estimated by summing the estimated image intensity histogram over the defined range.

The next image that we define is a “noise image” characterized by its low probability over the entire intensity band. Since the noise is essentially equally likely in each pixel, one approach to model it is to assume its probability is low relative to the other images. In this case we have found from our data base that

$$I(x, y) = a_n \ni 0 < a_n < 255 \text{ with } f_6 = \hat{p}_6 = \hat{H}(a_n) < \mathbf{0.2} \quad [\text{NOISE}] \quad (14)$$

Typical images that have fiducials created by alignment masks must also be classified and passed on to the pre-processor for off-normal condition detection. We call these images “valid” or “good” for further processing. This feature is defined by

$$I(x, y) = a_n \ni 0 < a_n < 255 \text{ with } f_7 = \hat{p}_7 = 1 - \sum_{k=1}^6 \hat{p}_k \geq \tau_{\text{prob}} \quad [\text{GOOD}] \quad (15)$$

Thus, with these models for each of the image types, we create a feature vector, $\mathbf{f} \in R^{7 \times 1}$ and construct the Bayesian-type classifier of the previous section, that is, we estimate each of the individual class probabilities from the given features, $\Pr(C_\ell | \mathbf{f})$, and then select the largest over all classes (blacks, white, noise, good) to determine the true class

$$\max \Pr(C_\ell | \mathbf{f}) \text{ for } \ell = 1, \dots, 7 \quad (16)$$

CLASSIFIER ALGORITHM

1. Transform the image to the 1D histogram function;
2. Estimate the feature vector component for each expected type of “off-normal” image specified above from Eqs. (13)-(15);
3. Choose the class (blacks, white, noise, good) based on the max $\Pr(C_\ell | \mathbf{f})$.

This completes the classifier-based, off-normal detector, next we investigate other features of more typical images assuming they have not been rejected by this detector using the above algorithm.

4. *Feature Detection Techniques*

In this section we develop procedures that are performed *after* the Bayesian-type classification has been performed to screen out the typical off-normal images. Here we actually have an image with the potential alignment mask (e.g. 2D gaussian pulse), but it could be distorted for a number of reasons discussed in the introduction. Thus, we have a valid image but it may possess “undesirable” features that would cause the alignment algorithm to give poor position estimate to the control loop. Our approach is the same, 2D \rightarrow 1D image transformation, but now we exploit properties of the beam quality that have been specified during the beam line design. From experience, we can allow a more liberal tolerance than the actual design specifications to perform the detection enabling a more robust performance of the detector.

a. *Full Width Half Maximum (FWHM) Detector*

In this sub-section we discuss the development of the FWHM off-normal detection technique, which proves to be very robust over our main laser beam beam lines. Again the major idea follows by transforming the image to two 1D functions, the row mean, \bar{I}_x , and the column mean, \bar{I}_y , defined by

$$\bar{I}_x(y) := \sum_{j=1}^{N_x} I(x_j, y_k); k = 1, \dots, N_y \text{ for } \bar{I}_x \in R^{N_y \times 1}$$

$$\bar{I}_y(x) := \sum_{j=1}^{N_y} I(x_j, y_k); j = 1, \dots, N_x \text{ for } \bar{I}_y \in R^{N_x \times 1}$$
(17)

Typically, these averages take the form of a pulse, either wide or narrow, depending on the 2D structure (e.g. 2D gaussian image \rightarrow 1D gaussian pulses); therefore, we define FWHM in the usual manner, that is,

$$I_{FWHM}(y) := \frac{1}{2} \bar{I}_x(y) \Big|_{y=y_n; y=y_m} \text{ for } y_n > y_m$$

$$I_{FWHM}(x) := \frac{1}{2} \bar{I}_y(x) \Big|_{x=x_n; x=x_m} \text{ for } x_n > x_m$$
(18)

From specifications for a given image, we know, a-priori, what the allowable interval or pulse width is for a given alignment loop. So we can define the respective allowable interval tolerances that are calculated from these values.

b. Full Width Half Maximum (FWHMP) Projection Detector

In this sub-section we discuss the development of the FWHMP off-normal detection technique, which can robustly handle the case where the 2D pulse shape is clipped at an angle. Again the major idea follows by transforming the image to two 1D functions, the angular row mean, $\bar{I}_{x\theta}$, and the angular column mean, $\bar{I}_{y\theta}$ where θ is the projection angle. In our case we limit the angle to the set, $\{0^\circ, 45^\circ, 90^\circ, 135^\circ\}$ where the 0° and 90° cases are precisely, $\bar{I}_{y0}(x) = \bar{I}_y(x)$ and $\bar{I}_{x90}(y) \equiv \bar{I}_x(y)$. In essence, we are only calculating two additional angular means, which are equivalent to calculating line integrals at particular projection angle similar to straight-line projection tomography.¹⁸

c. Pre-Processing

Many of the images have a varying intensity (bright-to-dim or dim-to-bright) depending on its illumination. This variation creates a trend in the projection data means; therefore, we remove it with a linear trend fit that is performed quite simply by locating the two endpoints of the 1D projection, creating the trend from the standard linear equation (slope is $\Delta y / \Delta x$, intercept is b). Typically, we actually define the endpoint 25 pixels in from the true endpoint to avoid any end effects created by the projection operation. Trend removal need not be perfect for the detection, since we only require the maximum location of the projection result.

This completes the discussion of the pre-processor used for off-normal detection, next we apply it to synthesized and actual measured images.

II. OFF-NORMAL DETECTION PERFORMANCE ON ENSEMBLE IMAGES

In this section, we discuss the application of the off-normal suite of 1D detection algorithms and demonstrate their performance on ensemble averaged off-normal images, that is, the test images are generated by a result of averaging an ensemble (> 30 members) of an alignment loop CCD camera output.

A. Classifier Performance

In this sub-section we investigate the performance of the classifier on a set of images to characterize its performance. A typical set of classifier outputs are shown in Fig. 2. We see in 2a and 2b that both the raw pure black and white images are easily detected and classified by their unique features. Note from the histogram estimates and feature probabilities, $\Pr(f_n | C_\ell)$, validate the classifications. In Fig. 2c and 2d we observe the linear mirror output, LM3, image as well as a small pinhole (gaussian-like pulse) in beam center and the large pinhole alignment image. These figures demonstrate strong normal black (f_4) and good (f_7) values, but in both cases the “good” feature is maximum and selected by the classifier.

After a number of runs, it was found that quite a number of valid or “good” images that could be processed were not selected by the classifier because of the large number of black pixels populating the image (e.g. small pinhole image) as illustrated in Fig 3a (MPAI) and 6b (Final Optics) images. We modified the feature selection by incorporating another constraint that sets its probability to zero if the probability threshold constraint is not satisfied. Compare the classifier outputs in Figs. 2 and 3. The effect of this approach demonstrated that it was possible to even correctly classify the black (or white) dominant images robustly as well. The results are clearly demonstrated in Fig. 3a-d. Note the black dominated KDP¹⁷ and Pinhole images are correctly classified by including this additional feature constraint. The classifier was also executed over an ensemble of 1000 all black images and was able to perform with less than 5% classification error (detection probability of >0.95) that is acceptable for this application because the subsequent off-normal tests are able to detect and reject the “bad” images.

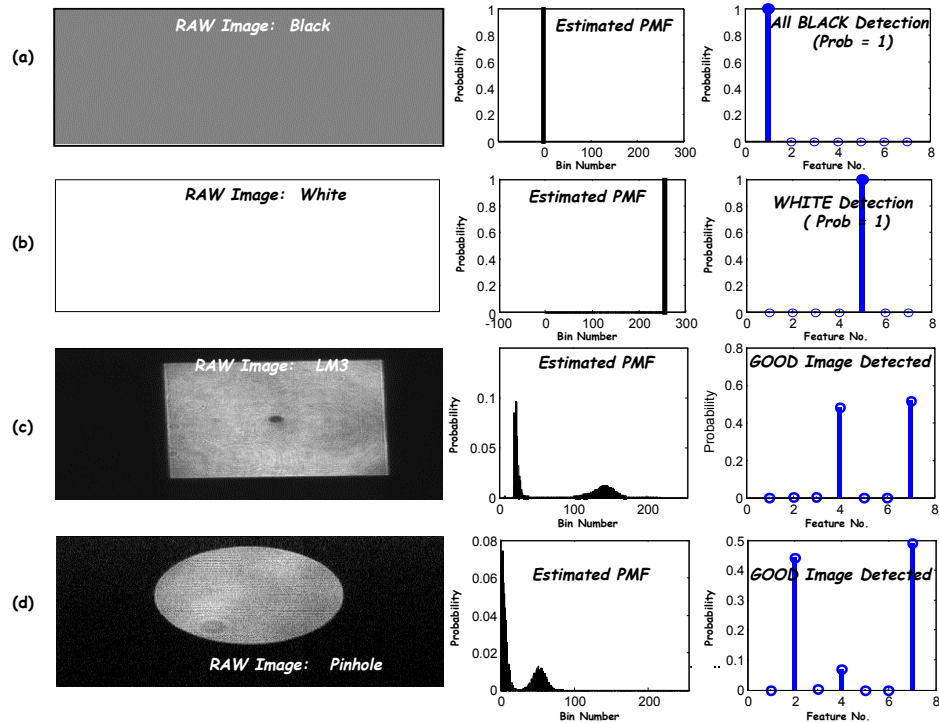


Fig. 2. Classifier outputs for: (a) Pure black image. (b) Pure white image. (c) LM3 image. (d) Pinhole image.

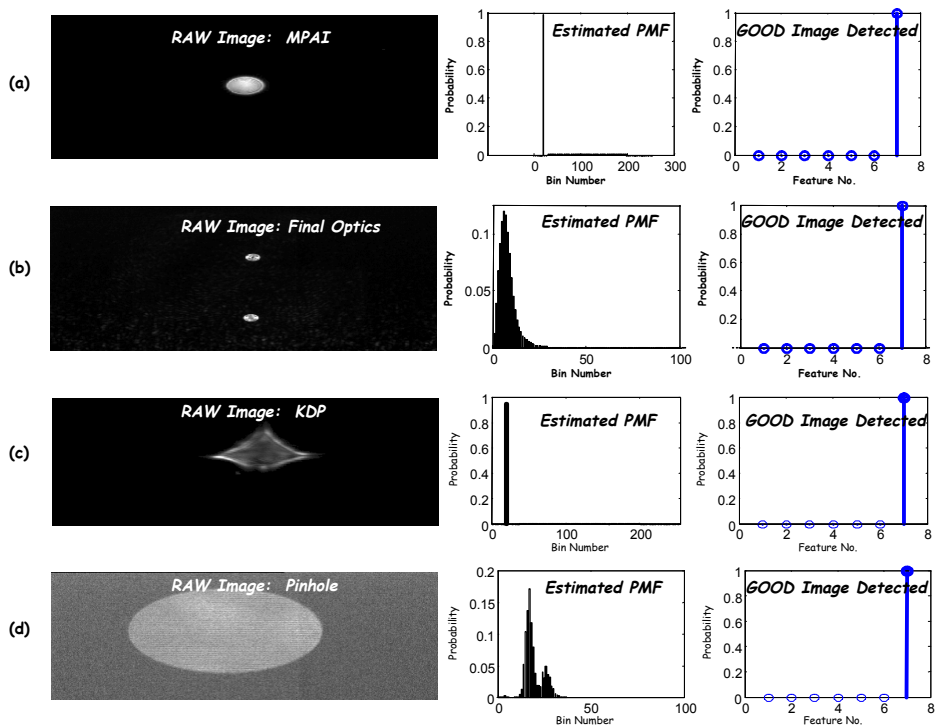


Fig. 3. Classifier outputs for: (a) MPAI image. (b) Final optics image. (c) KDP image. (d) Pinhole image.

B. Back-Lit Corner-Cube Reflection Images

The back-lit corner-cube reflection image is used in many beam lines to perform the alignment and eventual beam position estimation. A typical raw image (center box) is shown in Fig. 4 with the corresponding raw and processed row and column means. The image was acquired from the actual NIF beam line during “diagnostic” firing of the alignment laser. It consists of the ensemble average of 30-60 “shots” or firings. In this case, the beam was aligned with the reference successfully. The column mean has a distinguishable trend that is removed as part of the processing, while the row mean has a DC-offset that is also removed. The FWHM test was performed on these 1D functions indicating that the image was satisfactory for further processing.

Next we investigate the case of off-normal, corner-cube algorithms that are processed in much the same manner using the FWHM tests to detect any anomalies.¹⁹⁻²¹ The results for the “good” and “bad” images are shown in Fig. 5 where we see the raw images in the upper row followed by the column and row means after preprocessing. The first image was satisfactory and passed the FWHM tests while the other “clipped” images were rejected. Here the combined test was sufficient to reject these bad images. However, it was discovered that even if these tests were passed it was possible to still have bad images pass. This led to the development of the FWHMP that incorporates these tests including the additional 45° and 135° projections capable of robustly detecting this class of off-normal imaging.

This completes the section on the performance of the off-normal classification/detection algorithm suites with application to ensemble averaged images (reduced noise), next we apply the approach to actual noisy images and evaluate their overall performance.

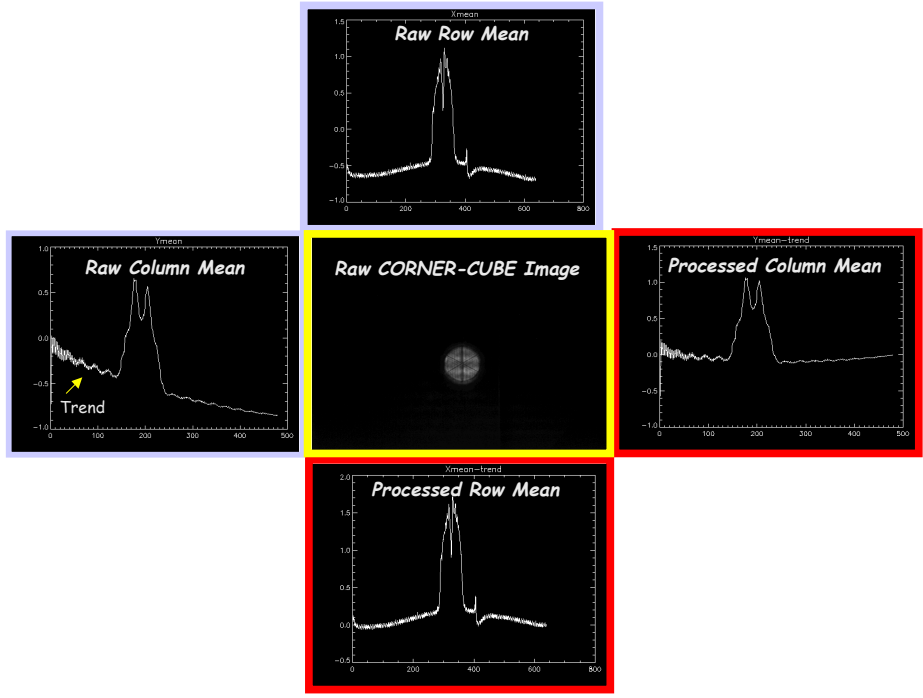


Fig. 4. Raw Corner-Cube Back Reflection Image and FWHM (2D \rightarrow 1D) Detection after pre-processing (trend removal).

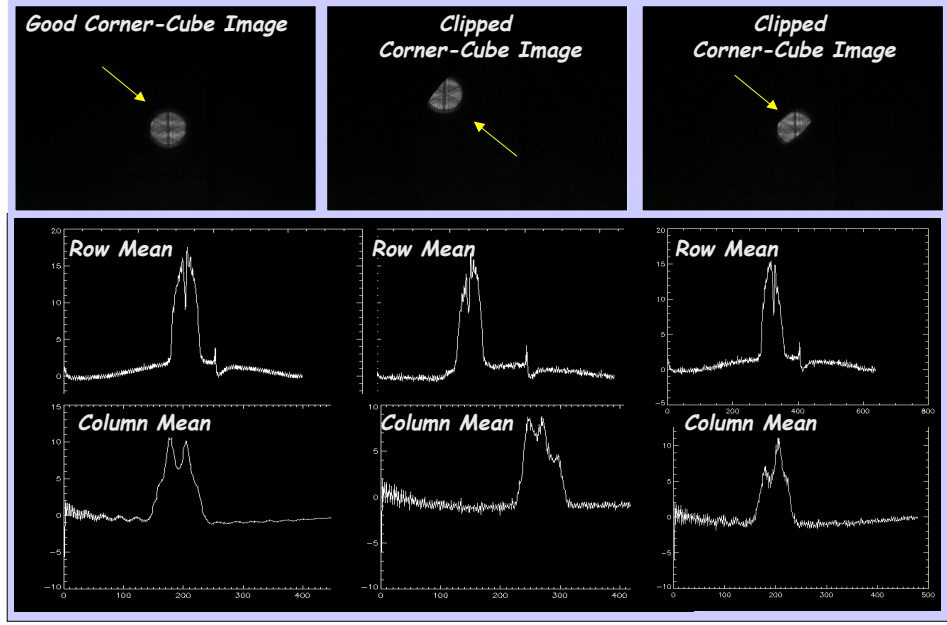


Fig. 5. Corner-Cube FWHM/Skewness Testing: Good and Clipped Images (pass, reject, reject).

III. OFF-NORMAL CLASSIFICATION/DETECTON RESULTS

In this section we discuss the application of the off-normal classifier/detector to a set of test images. The results are depicted in the subsequent table that demonstrate its performance.

We discuss a typical alignment loops. The loop alignment using back lit corner cube pinhole images. Table I describes the summarized results from a set of backlit-corner-cube-pinhole images that could be obtained during the operation of this loop caused by some opto-mechanical malfunction. Nominal images are shown in image number 1. They are circular with six diametrically placed lines at equi-angular positions. The last column of Tables I show whether an image *passes* as normal image by the off-normal preprocessor (termed *PP*). It also shows whether the algorithm is able to process the image as a normal image.

The criterion is based on a *tolerance threshold*, T ,

$$|L(\theta) - \mu_L| \leq T \quad (19)$$

for $L(\theta)$ the width (in pixels) of a line at angle, θ , which could be 0° , 45° , 90° or 135° and μ_L is the expected line width. Note that all four measurements along 0° , 45° , 90° , 135° must be within $T=20$ pixels of the expected width, otherwise it will be rejected by the preprocessor (*PP*).

Image number 1 is obtained by averaging 30 nominal images. The typical diameter of the image should be 78 pixels. However, since all the pinholes are situated on a single wheel, it is possible to have a different pinhole in the path, The second image is example of such off-normal condition. This case is rejected by the above criterion.

Another type of off-normal could result when the image of the pinhole is obstructed by the presence of a circular aperture in the path limiting its field of view. Image number, 3 shows such example. The X-FWHM and Y-FWHM widths together is not able to detect these cases. There are cases of image 4, where X-FWHM and Y-FWHM widths are calculated as 62 pixels, which are within 20 pixels of the expected size and accepted as a normal image. This prompted us to add the additional testing at 45 and 135 angles. Note that 135 angle was able to generate a condition favorable for rejection of image number 3.

It should also be pointed out that the back-lit corner-cube image is produced by two light sources superimposing the corner cube image to a common point. Ideally, the pointing direction is such that both sources produce images that appear to be a single image. When their pointing direction is not properly aligned, it is possible to have the two views of the corner cube image completely separate from each other as shown in images 4 of Table I. Note that this case produce a high Y-FWHM width value and are rejected.

Note that images 3-4 are all processed by the algorithm. However, the off-normal detector flags an uncertainty value of 640, which automatically shuts down the alignment loop. It forces the control operators to examine the image before letting the automatic alignment process continue. Thus with this arrangement of producing of high uncertainty given by the off-normal detector, the risk of mechanical failure is highly minimized.

This completes the illustration of the performance of the off-normal classifier/detector. Its performance over out alignment image suites has been outstanding as demonstrated by these runs.

TABLE I. NIF CONTROL LOOP No. 1 OFF-NORMAL DETECTOR PERFORMANCE.

Number	Image Loop Name	Detection Statistics	Result
1.	 A nominal image	X-FWHM WIDTH 71 Y-FWHM WIDTH 61 Crosswidth_45 67.88 Crosswidth_135 69.3 Expected_Size 78	PASS (PP,ALG)
2.	 A 150 micro-radian pinhole	X-FWHM width = 217 Y-FWHM width = 214 Crosswidth_1 = 183.848 Crosswidth_2 = 188.090 Expected_Size = 78	FAIL (PP)
3.	 A pinhole image obstructed by two mirrors	Skewness in X: -1.7207 Skewness in Y: -1.989 X-FWHM WIDTH 63 Y-FWHM WIDTH 53 Crosswidth_45 = 67.88 Crosswidth_135 = 48.08 Expected_Size 78	FAIL (PP) <i>Process(ALG)</i>
4.	 A double image produced by change in pointing direction of the two incident beams	X-FWHM WIDTH 69 Y-FWHM WIDTH 115 Crosswidth_45 = 89.1 Crosswidth_135 = 101.8 Expected_Size 78	FAIL (PP) <i>Process(ALG)</i>

IV. SUMMARY

We have developed an off-normal (image) classifier/detector based on the concept of transforming the original two-dimensional image to a one-dimensional function and extracting a variety of features that uniquely characterize each of the off-normal conditions. We developed a two-stage classifier/detector based on Bayesian classification principles. The design does not strictly adhere to the Bayesian formalism, since the appropriate conditional probabilities have not been estimated. However, the concept of features and their underlying probabilities have been exploited to develop an ad-hoc classification scheme coupled with a set of detection algorithms to determine off-normal images and inhibit their eventual processing. The performance of the classifier/detector has been investigated with great success on various ensembles of test images from the NIF data base. A 95% detection probability was achieved on the class of black images. We conclude from our processing that the classifier/detector is capable of correctly detecting off-normal images with high probability in this hostile environment.

ACKNOWLEDGMENT

We appreciate the technical advice and guidance from Dr. Erlan Bliss and Karl Wilhelmson of LLNL NIF Program during this study. This work was performed under the auspices of the U. S. Department of Energy by Lawrence Livermore National Laboratory under Contract No. W-705-Eng-48.

REFERENCES

1. D. Speck, E. Bliss, J. Glaze, J. Herris, F. Holloway, J. Hun, B. Johnson, D. Kuizenga, R. Ozarski, H. Patton, P. Ruppert, G. Suski, C. Swift and C. Thompson, "The Shiva laser-fusion facility," IEEE J. Quantum Electr., Vol. QE-17, No. 9, pp. 1599-1619, (1981).
2. J. Liu, H. Furuhashi, A. Torii, R. Sharma, V. Chitnis, B. Singh, J. Yamada, and Y. Uchida, "Automatic mask alignment in the theta direction using moiré sensors," Nanotechnology, **6**, pp. 135-138, (1995).
3. W. Blum, H. Kroha, P. Widmann, "A novel laser-alignment system for tracking detectors using transparent silicon strip sensors," IEEE Trans. Nuclear Sci., Vol. 43, No. 3, 1194-1199, (1996).
4. G. Seward, J. Leszczynski and E. Mulhern, "Rapid alignment of laser beams within optical systems," Opt. Eng., **36** (5), pp. 1414-1420, (1997).
5. A. Adolph, A. Boscheron, A. Dulac and E. Journot, "Final optics design for the megajoule laser," SPIE Proceedings, Vol. 3492, pt. 1-2, pp.44-50, (1999).
6. W. He, Q. Chen, R. Xu, Z. Peng, H. Yang, C. Zhu, and J. Zhao, "Image transfer based automatic alignment technique for laser-fusion facility," Acta Optica Sinica, Vol. 19, No. 9, pp. 1279-1283, (1999).
7. S. Roth, S. Schael, and G. Schmidt, "A test of the laser alignment system ALMY at the TTF-FEL," Nuclear Instr. Methods Phys. Res. A, Vol. 475, pp 537-544, (2001).
8. N. Fleurot, A. Adolf, M. Andre, J. Bruneau, C. Cavailler, M. Novaro, P. Philippe, F. Kovacs, B. Le Garrec, J. Di Nicola and J. Leidingner, "The ligne d'integration laser (LIL): construction status and first 1-w early results, Proc. SPIE, Vol. 4948, pp. 418-424, (2003).
9. D. Liu, J. Zhu, R. Zhu, D. Fan, "Laser beam automatic alignment in multipass amplifier," Opt. Eng., **43** (9), pp. 2066-2070, (2004).
10. R. Zacharias, N. Beer, E. S. Bliss, S. Burkhart, S. Cohen, S. Button, R. Van Atta, S. Winters, J. Salmon, M. Latta, C. Stoiz, D. Pigg and T. Arnold, "Alignment and wavefront control systems of the National Ignition Facility," Opt. Eng., **43** (12), pp. 2873-2884, (2004).
11. E. Moses, "The National Ignition Facility Comes to Life," Science & Technology Review, Lawrence Livermore National Lab. Report, pp. 4-14, Sept. (2003).
12. F. R. Holderner, E. Ables, E. S. Bliss, S. J. Boege, R. D. Boyd, C. J. Choccol, D. T. Davis, R. D. Demaret, R. E. English, C. W. Laumann, J. L. Miller and S. W. Thomas, "Beam control and diagnostic functions in the NIF transport spatial filter," Proceedings of SPIE 3047, Ed. Michel Andre, 692-699, (1996).
13. E. S. Bliss, F. R. Holderner, J. T. Salmon, J. R. Severyn, et. al., "Beam control and laser diagnostic systems," Lawrence Livermore National Lab. Report, UCRL-LR-105821-99-1, 79-97, (1999).
14. J. V. Candy, W. A. McClay III, A. A. S. Awwal, and W. Ferguson, "Optimal Centroid position estimation," in J. of Opt. Soc. Am., July 2005.
15. R. O. Duda, P. E. Hart and D. G. Stork, *Pattern Classification*, (John Wiley, New York, 2001).
16. A. Papoulis, *Probability, Random Variables, and Stochastic Processes*, (McGraw-Hill, New York, 1965)
17. A. Awwal, W. McClay, W. Ferguson, J. Candy, T. Salmon and P. Wegner, "Composite amplitude modulated phase-only filter based detection and tracking of the back-reflection of KDP images," in Photonic Devices and Algorithms for Computing VI, Eds. K. Iftekhjaruddin and A. A. S. Awwal, Proc. of SPIE **5556**, pp. 180-190, (2004).